Supplementary Information

Stacked Meshes with Super-Wettability via Atmospheric Plasma for Efficient Emulsion Separation

Zengyi He,[a,b] Linfeng Yang,[a,b] Xinpeng Cao,[a,b] Shan Zhou,[a] Lei Jiang[a,b] and Haoyu Dai*[a,b]

[a] CAS Key Laboratory of Bio-inspired Materials and Interface Science, Technical Institute of Physics and Chemistry, Chinese Academy of Sciences, Beijing 100190, China.

[b] School of Future Technology, University of Chinese Academy of Sciences, Beijing 100049, China.

* E-mail: daihaoyu@mail.ipc.ac.cn

Table of Contents

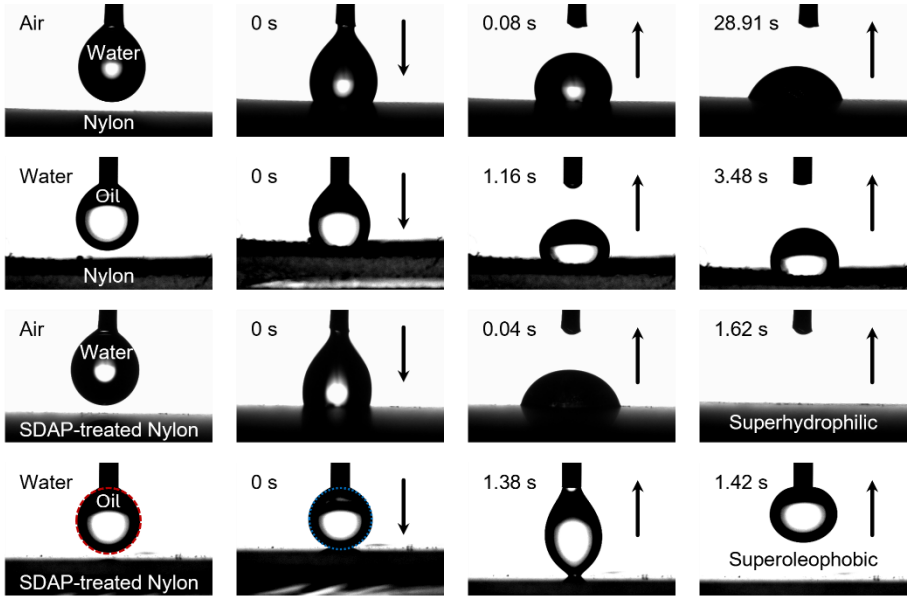

Fig. S1 The superhydrophilicity and ultra-low underwater oil adhesion of nylon mesh treated by surface diffuse atmospheric plasma (SDAP). The spreading and adhesion of water in air and oil in water on the surface of original nylon mesh and SDAP-treated nylon mesh, respectively. Compared to the original nylon mesh, water in air exhibits a faster spreading rate on the SDAP-treated nylon mesh surface. Oil underwater shows ultra-low adhesion on the SDAP-treated nylon mesh surface. As shown by the comparison of the red and blue frames, even after deformation caused by compression, the oil droplets can still detach from the nylon mesh.

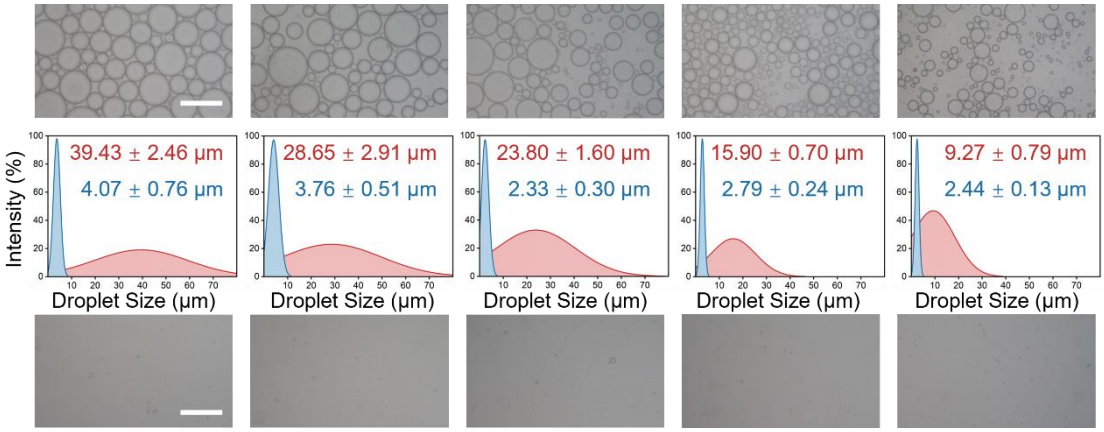

Fig. S2 The SDAP-treated nylon mesh exhibits excellent separation performance even for droplets smaller than the pore size. By analyzing the droplet diameters in micrographs before and after separation, it is evident that the SDAP-treated double-layer stacked nylon meshes effectively perform emulsion separation. After separation, the average droplet size in the filtrate is slightly smaller than the effective pore size of the double-layer stacked nylon meshes. Scale bar, 100 μm.

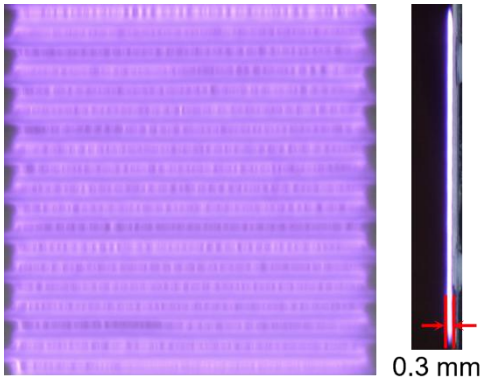

Fig. S3 The discharging state of SDAP. Optical image of SDAP in operation, showing bright purple glow from atmospheric plasma discharge with a plasma thickness of approximately 0.3 mm. The red box highlights a magnified view of the discharge region, primarily consisting of filamentary discharge paths between the electrodes.

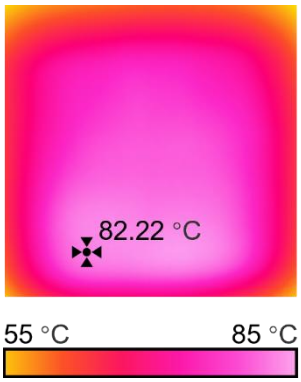

Fig. S4 The low-temperature characteristics of SDAP discharge. The infrared image of SDAP shows a maximum temperature of 82.22°C.

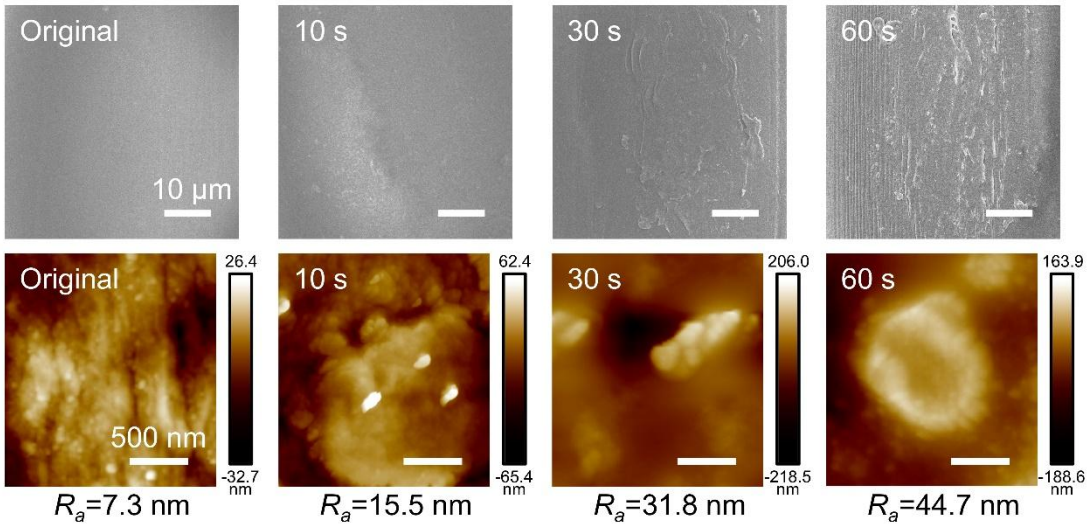

Fig. S5 Scanning electron microscope (SEM) images and atomic force microscope (AFM) images of nylon mesh treated by SDAP with different time. With the increase of SDAP treatment time, the surface of nylon fibers showed obvious micro-nano structure and the roughness increased.

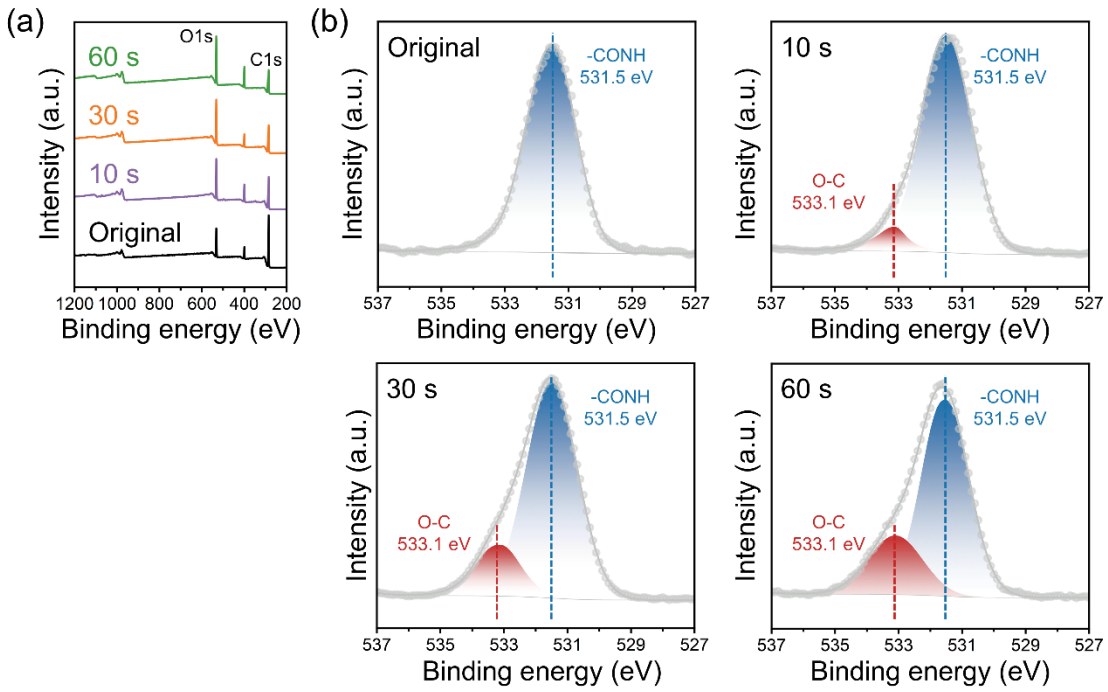

Fig. S6 X-ray photoelectron spectroscopy (XPS) and peak-fitted high-resolution O 1s spectra of nylon mesh treated by SDAP with different time. (a) XPS full spectra of nylon mesh treated by SDAP with different time. (b) Peak-fitted high-resolution O 1s spectra of nylon mesh treated by SDAP with different time. As the SDAP treatment time increased, more and more newly generated O-C was observed. Due to the similarity in binding energy, the newly formed O=C peak is enveloped by the pre-existing -CONH peak. Relative contents of the elements and deconvolution analysis of O 1s peaks of nylon mesh treated by SDAP with different time are shown in Table S1.

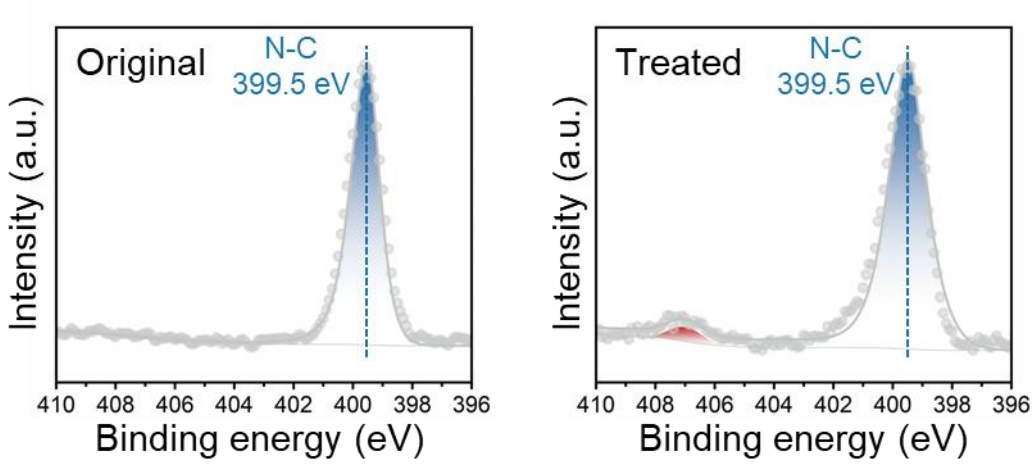

Fig. S7 Peak-fitted high-resolution N 1s spectra of original and SDAP-treated nylon meshes. In the high-resolution N 1s spectra of SDAP-treated nylon mesh, a new peak can be observed indicating the generation of a high-valent nitrogen salt.[1]

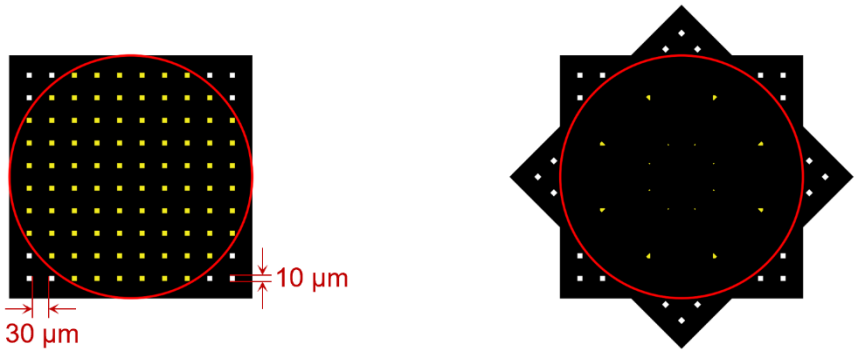

Fig. S8 Calculation of effective pore size of multi-layer stacked nylon meshes in the horizontal direction. The number of stacked layers increases sequentially from left to right, following the principle of uniform stacking. The black wireframe is nylon fiber, and the area of the yellow area inside the red tangent circle is the transmission area (S) of emulsion using the CAD software statistics, the number of holes is N, and the equivalent square pore diameter d is calculated based on this information. It can be calculated by the formula S1, where the corresponding S, N and d at the number of stacked layers are shown in Table S2.

$$d = \sqrt{S/N} \tag{S1}$$

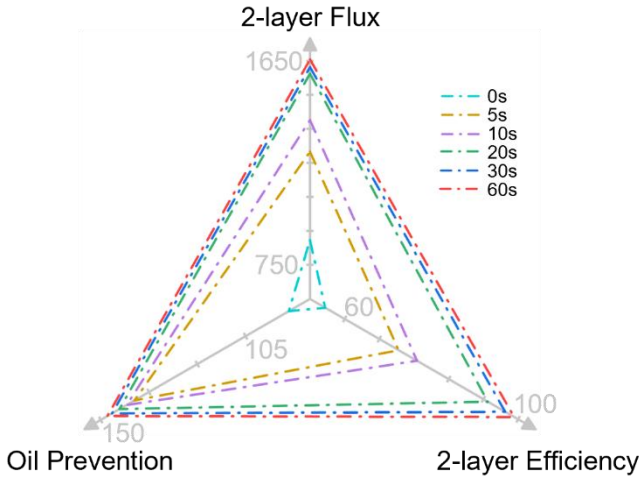

Fig. S9 Emulsion separation characteristics of nylon mesh treated by SDAP with different time. The SDAP-treated nylon mesh exhibited significant improvements in three aspects: underwater oil resistance, double-layer separation efficiency, and double-layer separation flux.

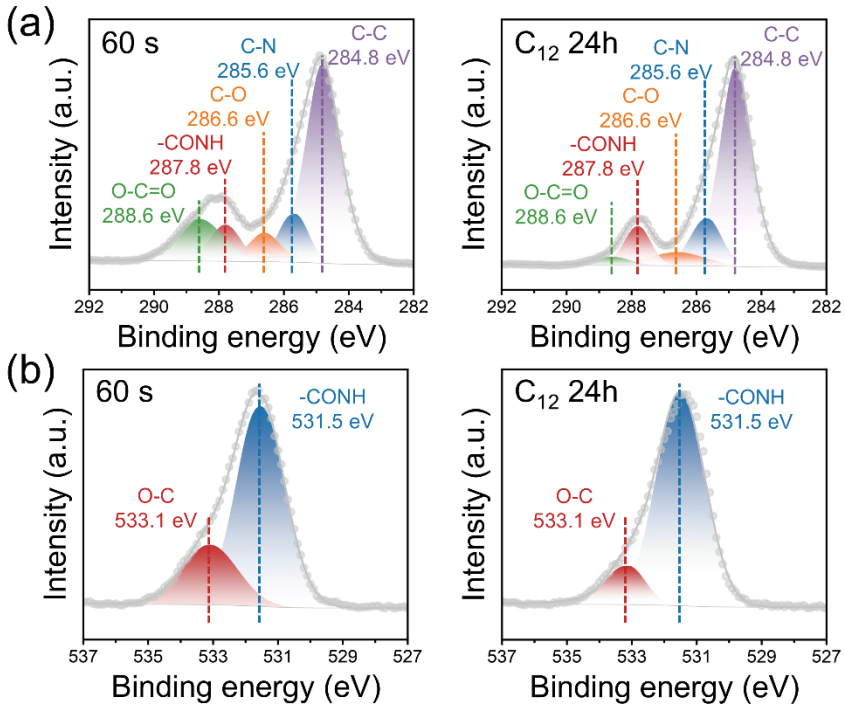

Fig. S10 Peak-fitted high-resolution C 1s and O 1s spectra of nylon mesh treated by SDAP with 60 s placed in n-dodecane for 24 h. (a) Peak-fitted high-resolution C 1s spectra. (b) Peak-fitted high-resolution O 1s spectra. Immersion in n-dodecane resulted in a reduction of C-O and other oxygen-containing functional groups on the surface of the SDAP-treated nylon mesh, which was the main reason for the hydrophilicity decline of the nylon mesh after multiple emulsion separation cycles. Deconvolution analysis of C 1s and O 1s peaks of nylon mesh treated by SDAP with 60 s placed in n-dodecane for 24 h are shown in Table S3.

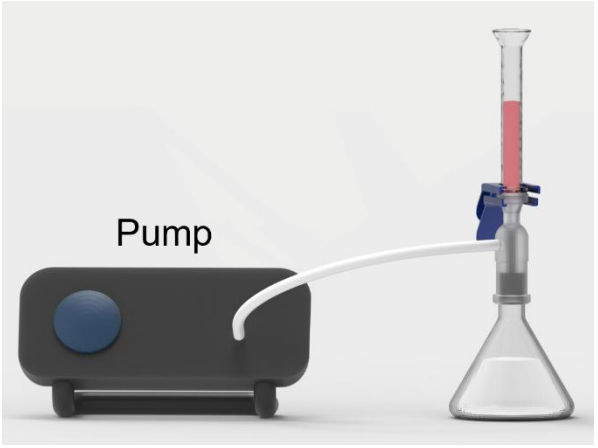

Fig. S11 Schematic of apparatus for evaluating the oil intrusion resistance during emulsion separation. A suction pump actively drives the emulsion separation process through the SDAP-treated nylon mesh, allowing for adjustable permeation pressure compared to gravity-driven separation. This setup is used to test the oil intrusion resistance of the SDAP-treated nylon mesh.

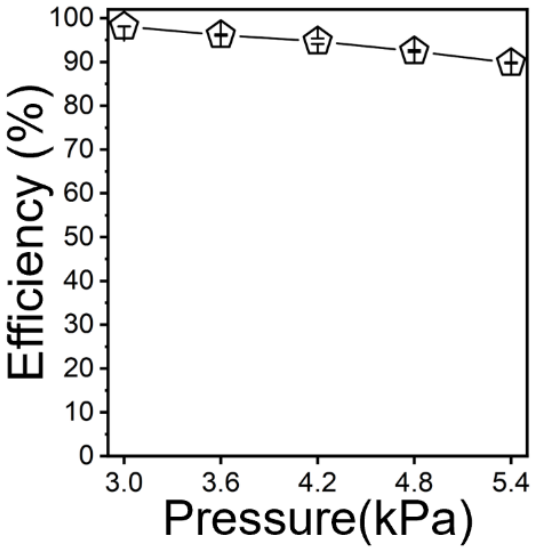

Fig. S12 The test of evaluating the oil intrusion resistance during emulsion separation. In the emulsion separation process, the oil intrusion resistance of the nylon mesh was validated by artificially increasing the permeation pressure. The results showed that even with an 80% increase in pressure, a 90% separation efficiency was maintained. This characteristic makes the SDAP-treated nylon mesh more suitable for complex working conditions in practical applications.

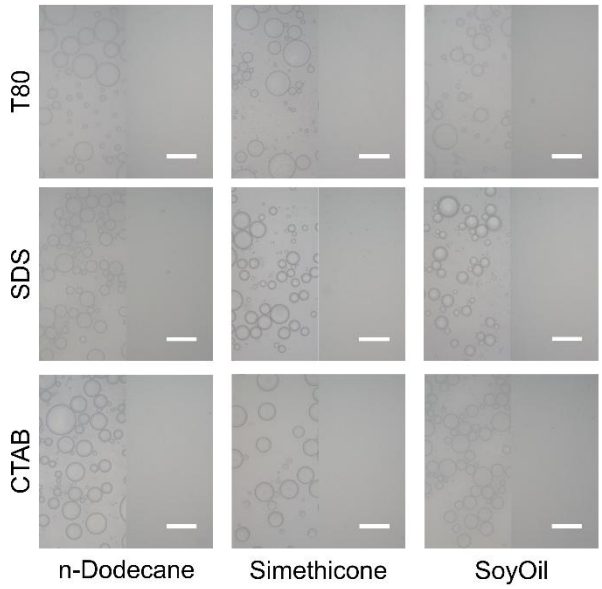

Fig. S13 The separation performance of 2-layer nylon meshes treated by SDAP for 30 s for emulsions formulated with different oil phases combined with various surfactants. Optical microscope image comparison of emulsions composed of different kinds of oils and surfactants before and after separation. Scale bar, 100 μm.

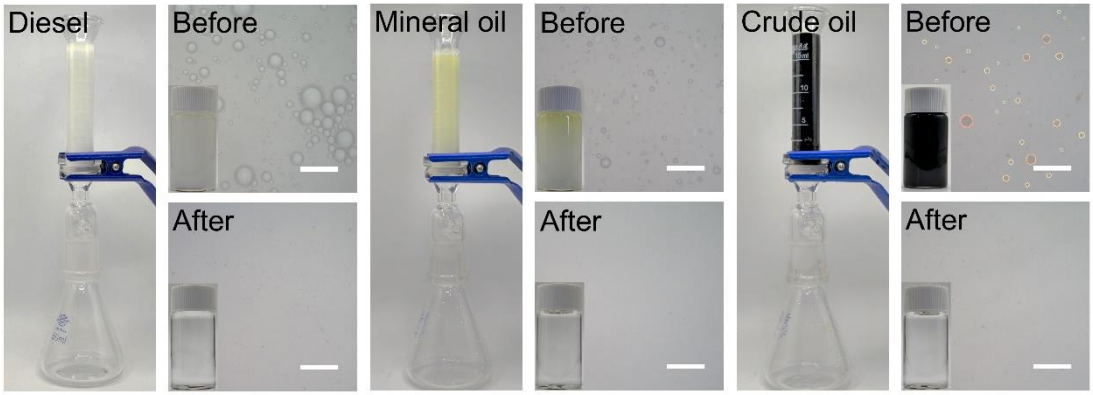

Fig. S14 The separation performance of 2-layer nylon meshes treated by SDAP for 30 s for emulsions formulated with different oil phases. Photographs of emulsions composed of different types of oils before and after separation were compared with the corresponding optical microscope images. Scale bar, 100 μm.

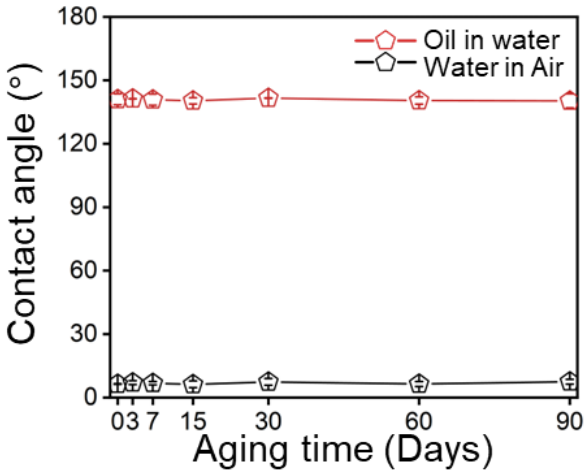

Fig. S15 Aging test in air of SDAP-treated nylon mesh. The water contact angle in air and oil contact angle in water of SDAP-treated nylon mesh when stored in air for 90 days.

Table S1 Relative contents of the O element and deconvolution analysis of O 1s peaks of nylon mesh treated by SDAP with different time.

	Original (%)	10 s (%)	30 s (%)	60 s (%)		Original (at.%)	10 s (at.%)	30 s (at.%)	60 s (at.%)
O/C	21.5	42.0	50.0	54.6	-CONH	100	90.61	82.06	74.15
					O-C	0	9.39	17.94	25.85

Table S2 The corresponding S, N, d at the number of stacked layers.

Stack Number	S (μm^2)	N	d (μm)
1	8800	88	10.00
2	566.6658	16	5.95
3	~0	~0	~0
4	~0	~0	~0
5	~0	~0	~0

Table S3 Deconvolution analysis of C 1s and O 1s peaks of nylon mesh treated by SDAP with 60s placed in n-dodecane for 24 h.

	60 s (at.%)	C_{12} 24 h (at.%)		60 s (at.%)	C_{12} 24 h (at.%)
C-C	57.02	64.29	-CONH	74.15	86.54
C-N	11.39	15.09	O-C	25.85	13.46
-CONH	8.66	10.47			
C-O	7.67	7.15			
O-C=O	15.26	3.01			

Table S4 Comparison of other studies of the same type with this study.

Material	Emulsions Type	Maximum Flux ($L \cdot m^{-2} \cdot h^{-1} \cdot bar^{-1}$)	Separation Efficiency (%)	Time For Preparation (s)
2D $Ti_3C_2T_x$ MXene membrane[2]	O/W	887	>99.0	5.4×10^4
CNTs-based membranes[3]	O/W	1660	>86.5	3.2×10^5
Adhesive hydrogel decorated membrane[4]	O/W	1720	>99.9	1.8×10^5
PVDF/PHEMA membrane[5]	O/W	1756	>99.8	1.7×10^5
PVDF/PDA/PACMO membrane[6]	O/W	1800	>99.8	2.0×10^5
Polypropylene membranes[7]	O/W	3548	>99.0	1.5×10^4
GO/SiO_2 membrane[8]	O/W	4550	>99.0	3.6×10^2
Nanocellulose-based membrane[9]	O/W	29003	>99.8	4.1×10^5
Co_3O_4 nano-needle mesh[10]	O/W	40000	>99.0	3.2×10^4
Biomimetic composite nanofibrous membrane[11]	O/W	45280	>99.0	6.4×10^4
This work	O/W	56356	98.9	60

References

1 L. Yang, J. Sun, Z. He, D. Hao, Y. Feng, H. Dai and L. Jiang, *RSC Adv.*, 2024, **14**, 18073-18079.

2 H. Zhang, Z. Wang, Y. Shen, P. Mu, Q. Wang and J. Li, *J. Colloid Interface Sci.*, 2020, **561**, 861-869.

3 Y. Gu, H. Li, L. Liu, J. Li, B. Zhang and H. Ma, *Carbon*, 2021, **178**, 678-687.

4 S. Gao, J. Chen, Y. Zheng, A. Wang, D. Dong, Y. Zhu, Y. Zhang, W. Fang and J. Jin, *Adv. Funct. Mater.*, 2022, **32**, 2205990.

5 Y. Wang, H. Yang, Y. Yang, L. Zhu, Z. Zeng, S. Liu, Y. Li and Z. Liang, *Sep. Purif. Technol.*, 2022, **285**, 120298.

6 Y. He, K. Xu, X. Feng, L. Chen and Z. Jiang, *J. Membr. Sci.*, 2021, **637**, 119644.

7 H. Yang, J. Pi, K. Liao, H. Huang, Q. Wu, X. Huang and Z. Xu, *ACS Appl. Mater. Interfaces*, 2014, **6**, 12566-12572.

8 J. Sun, H. Bi, S. Su, H. Jia, X. Xie and L. Sun, *J. Membr. Sci.*, 2018, **553**, 131-138.

9 J. Wu, Y. Su, Z. Cui, Y. Yu, J. Qu, J. Hu, Y. Cai, J. Li, D. Tian and Q. Zhang, *Nano Res.*, 2023, **16**, 5665-5675.

10 Y. Chen, N. Wang, F. Guo, L. Hou, J. Liu, J. Liu, Y. Xu, Y. Zhao and L. Jiang, *J. Mater. Chem. A*, 2016, **4**, 12014-12019.

11 J. Ge, D. Zong, Q. Jin, J. Yu and B. Ding, *Adv. Funct. Mater.*, 2018, **28**, 1705051.